AGU ADVANCING EARTH AND SPACE SCIENCE

Geophysical Research Letters

RESEARCH LETTER
10.1029/2021GL097690

Turbulent Mixing in the Barrier Layer of the Equatorial Pacific Ocean

Chuanyu Liu[1,2,3,4], Dan Huo[1,2], Zhiyu Liu[5], Xiaowei Wang[1,3,4], Cong Guan[1,3,4], Jifeng Qi[1,2,3,4], and Fan Wang[1,2,3,4]

[1]CAS Key Laboratory of Ocean Circulation and Waves, Institute of Oceanology, Chinese Academy of Sciences (IOCAS), Qingdao, China, [2]College of Earth and Planetary Sciences, University of Chinese Academy of Sciences (UCAS), Beijing, China, [3]Marine Dynamic Process and Climate Function Laboratory, Pilot National Laboratory for Marine Science and Technology (Qingdao) (QNLM), Qingdao, China, [4]Center for Ocean Mega Science, Chinese Academy of Sciences, Qingdao, China, [5]State Key Laboratory of Marine Environmental Science, and Department of Physical Oceanography, College of Ocean and Earth Science, Xiamen University, Xiamen, China

Key Points:

- Direct turbulence measurements and data-based mixing estimates reveal high occurrence of BL mixing in the western-central equatorial Pacific
- BL mixing is associated with significant cooling, salting, and deepening of the mixed layer, and cooling, salting, and weakening of the BLs
- The frequent BL mixing shows regular seasonal and interannual variations and may impact the El Niño development via modulating SSTs

Supporting Information:

Supporting Information may be found in the online version of this article.

Correspondence to:

C. Liu and F. Wang,
chuanyu.liu@qdio.ac.cn;
fwang@qdio.ac.cn

Citation:

Liu, C., Huo, D., Liu, Z., Wang, X., Guan, C., Qi, J., & Wang, F. (2022). Turbulent mixing in the barrier layer of the equatorial Pacific Ocean. *Geophysical Research Letters*, *49*, e2021GL097690. https://doi.org/10.1029/2021GL097690

Received 6 JAN 2022
Accepted 10 FEB 2022

Abstract The barrier layer (BL) is an expansive halocline layer commonly found in the western equatorial Pacific, long been thought to inhibit entrainment of colder thermocline water into the surface mixed layer (ML), consequently facilitating the development of El Niño. But here we find frequent turbulent mixing in the BL from both direct turbulence measurements and indirect mixing estimates within an 11-year-long Argo profile data set. The observed BL mixing is as strong as in the ML, yielding effective heat transfers across the isothermal layer (IL) base. The estimated BL mixing is ubiquitous, with occurrence ranging 20%–60% spatially and peaking at around 160°W, 0°N; it occurs more frequently in La Niña than El Niño years. The BL mixing is associated with thicker ML, BL, and IL, weaker BL stratification, and lower temperature and higher salinity in the IL. How the BL mixing may impact the El Niño development deserves further exploration.

Plain Language Summary The vertical structure of the subsurface layer in the western equatorial Pacific Ocean is unique because of heavy rainfall. There, the temperature mixed layer extends from surface to a higher depth (typically 50–80 m) while the surface density mixed layer is usually confined to a lower depth (typically 20–30 m). The 20–60 m-thick layer in-between is a halocline layer. The presence of the halocline layer can prevent entrainment of cold deeper water into the warmer surface layer, thus inhibiting cooling of the surface water and helping maintain shallow surface mixed layers. Therefore, the halocline layer is called barrier layer (BL). One of the thermodynamic consequences of the BL is that the sustained shallow mixed layers favor quick responses to wind and regular onset of El Niño events. However, in the present study, we find evidences that the BLs are associated with frequent turbulence mixing that can greatly reduce or even destroy the BLs. The finding of frequent BL mixing is unanticipated. It suggests that the BL mixing may impact the development and magnitude of El Niño via changing BLs' intensity, and thus influence both the global and regional climates, which, however, remains unrevealed and demands further exploration.

1. Introduction

The upper western equatorial Pacific Ocean is characterized by a peculiar vertical thermohaline structure. There, the mixed layer for temperature (usually termed as the isothermal layer, IL, typically 50–80 m thick) usually extends well below the mixed layer for density (ML, typically 20–30 m thick). The 20–50 m thick layer between the ML and IL bases is a halocline-induced weakly stratified layer known as the barrier layer (BL) (Ando & McPhaden, 1997; Lukas & Lindstrom, 1991; Sprintall & Tomczak, 1992).

The presence of BL has significant thermodynamic and dynamic consequences. In the tropical oceans, the sea surface temperature (SST) is the agent of ocean's impact on the atmospheric circulation. Lukas and Lindstrom (1991) hypothesized that the BL would inhibit entrainment cooling of the surface layer. Model simulations confirmed that the warm pool BLs act to maintain shallow MLs and warm SSTs by isolating the ML from entrainment cooling in the IL base (Maes et al., 1997; Vialard and Delecluse, 1998a, 1998b; Vialard et al., 2001; Vialard et al., 2002). Furthermore, the sustained shallow MLs favor enhanced and quick responses to wind (Maes et al., 2002; 2005). A particularly important dynamical consequence of BL is to modulate the development of El Niño (Corbett et al., 2017; Guan et al., 2019; Maes and Belamari, 2011; Maes et al., 2002; 2005; Qu et al., 2014; Zheng et al., 2014). Maes et al. (2002, 2005) demonstrated that the removal of BL in the warm pool

by artificially introduced strong mixing leads to cooling of sea surface, deepening of the ML, westward shrinking of the warm pool and subsequently reduced fetch of westerly wind anomalies, which ultimately prevents development of El Niño. In addition, the BL affects another necessary condition for El Niño's development, that is, the buildup of anomalous warm water volume (WWV) over the upper part of the tropical Pacific Ocean (Jin, 1997; McPhaden, 2002; Meinen & McPhaden, 2000; Wyrtki, 1975). Those results revealed that the BL is one of the key elements of the El Niño and southern oscillation (ENSO) and the ocean-atmosphere-coupled system.

To summarize, Maes et al.'s sensitivity studies (Maes et al., 2002; 2005; Maes and Belamari, 2011) have two implications. On the one hand, the presence of BL is essential for the development of El Niño, which has also been confirmed by other studies as mentioned above. On the other hand, mixing in the BL, if there is, is also important for the development of El Niño. However, in the previous coupled model-based sensitivity studies, one usually assumed very strong mixing in the BL (so that the BL is artificially destroyed) in the warm pool region and the strong mixing lasts for a continuous long time period. It can be easily envisioned that if the mixing in the BL is moderate or weak, or varies with time, the coupled model may evolve differently.

However, whether BL mixing indeed exists in the warm pool or in the other regions of the equatorial Pacific remains unrevealed. It is also unknown whether the mixing varies with time and space. The reason why few efforts have been made to identify the BL mixing and its variation is probably due to difficulty in turbulence measuring in the past. In the present study, we will present the existence of BL mixing in the equatorial Pacific. We first report on the occurrence of turbulent mixing in the BL with direct turbulence measurements in the western equatorial Pacific; we then present all possible BL mixing events during a long time period (2010–2020) in the tropical Pacific with indirect mixing estimates from Argo profile data set. (In the past decade, Argo profiles have been widely used in estimating diapycnal mixing in the global oceans, particularly based on the Fine Scale Parameterization method, e.g., Whalen et al., 2018.) Here, we employ a different method to determine the mixing events. The spatial and temporal variations of the mixing events, and the conditions that are associated with and without BL mixing are also investigated. Those results are presented in Section 3, following an introduction of Method in Section 2.

2. Method

The direct turbulence measurements analyzed in this study were carried out during two 3-day long intensive profiling experiments at 142°E, 0°N during 15–18 December, 2017 (Experiment I), and 158°E, 0°N during 6–9 January, 2019 (Experiment II). During both experiments, the turbulent kinetic energy (TKE) dissipation rate, ϵ, was obtained every 2 h using a vertical microstructure turbulence profiler (VMP, Rockland Scientific) with a shear probe of 5% accuracy. The turbulence diffusivity k of each profile is estimated from ϵ according to $k = \Gamma\epsilon/N^2$, where $N^2 = -g\partial\rho/(\rho_0\partial z)$, ρ_0 (=1020 kg m^{-3}) is a reference density, g is the acceleration due to gravity, ρ is calculated from sorted density and $\Gamma = 0.2$ is a canonical value of the mixing efficiency factor (Osborn, 1980).

Standard temperature, salinity, pressure, and velocity data were profiled in-between the VMP casts using an assembly of a Conductivity-Temperature-Depth (CTD, SBE37, accuracy is 0.003°C for temperature and 0.02 PSU for salinity) and a Lowered Acoustic Doppler Current Profiler (LADCP, with precision of 1.0%). Furthermore, the mean heat flux (J_q) due to turbulent mixing during the experiment is estimated as $J_q = -\rho_0 C_p \langle k \rangle \ \partial\langle T \rangle/\partial z$, where T is temperature, $C_p \left(= 4060 \ J \ kg^{-1} \ K^{-1}\right)$ is heat capacity of sea water, and $\langle * \rangle$ denotes an experiment-average. Analogously, the mean salinity flux due to turbulent mixing is estimated as $F_s = -\langle k \rangle \partial\langle S \rangle/\partial z$, with S the salinity.

In addition, in order to determine how frequent the BL mixing occurs, and how it varies with regions and time, we adopt the Thorpe Scale methodology (Thorpe, 1977) to the long-term (2010–2020), widely covered Argo profiles with a vertical grid spacing of 2 m or less, to detect mixing events that are represented by density inversions (overturns) in the BL. Note that we did not use this method to estimate mixing coefficients, but only detect the mixing events. A mixing event is determined only when the overturn patch covers three or more consecutive grid points along the vertical and it was lying in the BL. Due to this criterion and the low resolution of Argo profiles, smaller-scale mixing events are not detected. Note that prior quality-control processes have been made to the Argo profiles to make the identification of overturns possible.

The profiles with and without detected mixing events in the BL are denoted as "BL mixing" and "BL non-mixing" profiles, respectively. We then calculate the occurrence of BL (r_{BL}) and BL mixing ($r_{\varepsilon T}$), where r_{BL} is the ratio of the number of profiles with BL to the number of all qualified profiles, while $r_{\varepsilon T}$ is the ratio of the number of profiles with BL mixing to the number of profiles with BL, over a certain area and time period.

In this study, the IL is defined such that the temperature at the IL base is 0.2°C lower than the near-surface (at 10 m depth) temperature (de Boyer Montégut et al., 2004), and the ML is defined such that the density at the ML base is 0.01 kg/m^3 lower than the near-surface (also at 10 m depth) value (Schneider & Muller, 1990). Finally, the layer between the ML and the IL bases is defined as the BL (Lukas & Lindstrom, 1991), as long as it meets the following additional conditions: (a) the layer thickness is larger than two times the vertical resolution; (b) the layer-averaged haline part of N^2 (i.e., the salinity-associated squared buoyancy frequency, $N^2(S)$) is positive and accounts for more than 30% of the N^2, where $N^2(S) = N^2 - N^2(T)$, $N^2(T) = g\alpha\partial T/\partial z$, and α is the thermal expansion coefficient, following an idea of Maes and O'Kane (2014).

3. Results

3.1. Observational Evidence of BL Mixing

Here, we report on the occurrence of BL mixing from turbulence measurements (Figure 1). First, BLs were prominent in both experiments (Figure S1 in Supporting Information S1), with the experiment-averaged BL thickness being about 25 and 65 m, respectively (Figures 1c and 1h). Second, both experiments revealed evident turbulent mixing patches in the BLs (Figures 1a and 1f; e.g., 15 December, 2:00–16 December, 12:00, and 17 December, 0:00–12:00 of Experiment I, and 6 January, 21:00–7 January, 9:00 and 8 January, 9:00–21:00 of Experiment II). The magnitude of ϵ in the BL over Experiment I was 10^{-6}–10^{-7} W/kg, comparable to that in the ML; it was 10^{-7}–10^{-8} W/kg over Experiment II, when ML mixing was confined to the upper 15 m (Figures 1d and 1i). During Experiment I, the ML mixing and BL mixing appeared to affect each other for the first-half period but well separated afterward. During Experiment II, the BL mixing was well separated from the ML mixing over the entire experiment. Over both the experiments, the BL mixing spanned from the lower range of the BL to the top layers of the thermocline, that is, approximately 10 m deeper than the BL bases. It is noticed that Experiment I experienced a strong northwesterly, with experiment-averaged zonal wind speed of 6.8 m s^{-1}, about six times greater than the monthly climatology of 1.0 m s^{-1} at this site for December (based on 2008–2019 ASCAT data), while Experiment II experienced a light wind condition, with experiment-averaged wind speed of 1.8 m s^{-1}, not much different from its monthly climatology of 1.1 m s^{-1} for January.

The resulting k was largest in the upper ML (Figures 1b, 1d and 1g and 1i), with a magnitude up to 10^{-2} m^{2}s^{-1}. It was decreased to 10^{-4}–10^{-3} m^{2}s^{-1} in the BL layer of Experiment I, comparable to the lower ML and larger than the thermocline layer further below. It was 10^{-5}–10^{-4} m^{2}s^{-1} in the BL of Experiment II, higher than the lower ML.

The experiment-averaged J_q (Figures 1e and 1j) ranged from 0 to 20 Wm^{-2} for Experiment I and 0 to 50 Wm^{-2} for Experiment II. Note that because mixing extended downward from BL to the upper thermocline, it enabled heat exchanges between those two layers. The heating/cooling rate of a fluid parcel due solely to diapycnal/vertical mixing can be determined by the one-dimensional vertical diffusion equation, that is, $\frac{\partial T}{\partial t} = -\frac{1}{\rho_0 C_p}\frac{\partial J_q}{\partial z}$ (t is time); the depth of the maximum J_q determines the point separating heating and cooling. J_q maximum of both experiments peaked near the BL bases, therefore, large vertical divergence (convergence) of J_q contributed to cooling (heating) of the lower layers of the BL (top layers of the thermocline), with an average rate of −0.54 K/month (+0.47 K/month) for Experiment I, and −0.20 K/month (+0.89 K/month) for Experiment II. Ignoring other processes, the BL mixing-induced cooling in the bottom of BL (also the bottom of IL), may ultimately be felt by the whole IL due to upper layer mixing processes, and leads to cooling of the ML. Here the upper layer mixing processes could include the coherent ML/BL mixing seen in the first-half period of Experiment I.

The experiment-averaged F_s (Figures 1e and 1j) ranged between 0 and -4.2×10^{-6} (0 and -1×10^{-6}) PSU ms^{-1} for the two experiments, respectively, reaching maximum also near the IL bases. These vertical patterns lead to a mean salting (freshening) rate in the BL (upper thermocline) of +0.02 PSU/month (−0.01 PSU/month) for Experiment I, and +0.03 PSU/month (−0.09 PSU/month) for Experiment II. (Note that a second peak of F_s

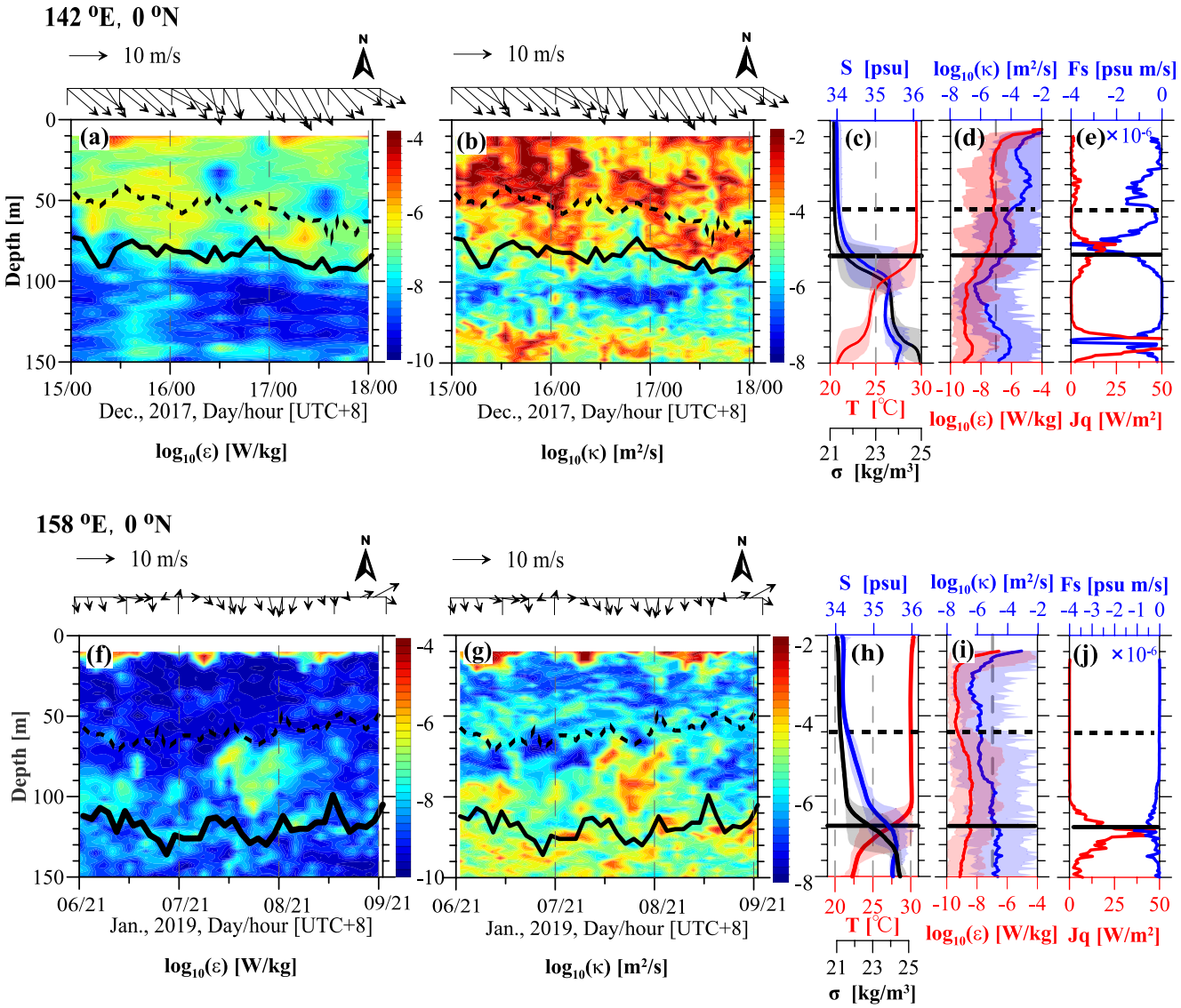

Figure 1. (a)–(e) Experiment I; (f)–(j) Experiment II. (a), (f), ϵ in a logarithm scale, accompanied with wind; the thick and dashed lines denote the IL and ML bases, respectively; between them is the BL. (b), (g), diffusivity k; (c), (h), experiment-averaged potential temperature T, salinity S, potential density σ; shading areas denote max- and min-range. (d), (i), experiment-averaged ϵ and k in logarithm scales; (e), (j), experiment-averaged turbulence heat flux J_q and salinity flux F_s (note the different axis ranges between e and j). See Section 2 for calculation. In the right three columns, black dashed and solid level lines denote the experiment-averaged IL and ML bases, respectively.

occurred just above the MLD during Exp. I, which also resulted in salting/freshening nearby the MLD.) The BL mixing-induced salting (freshening) of the BL (upper thermocline) decreased the stratification over the BL/upper thermocline layers.

3.2. Detection of BL Mixing From the Argo Profiles

The Argo profiles confirm that BL is a prominent feature of the western equatorial Pacific Ocean (Figure 2a), with r_{BL} being over 90% in the Western Pacific Warm Pool (which roughly lies west of 170°E; e.g., Maes et al., 2005); r_{BL} decreases eastward along the equatorial band (Figures 2a and 2c). These results are consistent with previous studies (Bosc et al., 2009; Delcroix et al., 1992; Maes & O'Kane, 2014). In the western equatorial Pacific where BL frequently takes place, for example, 140°E–180°, 5°S–5°N (blue box in Figure 2a), the r_{BL} shows a weak annual cycle (Figure 2d), which is maximum in early boreal summer (82%) and minimum in October (70%).

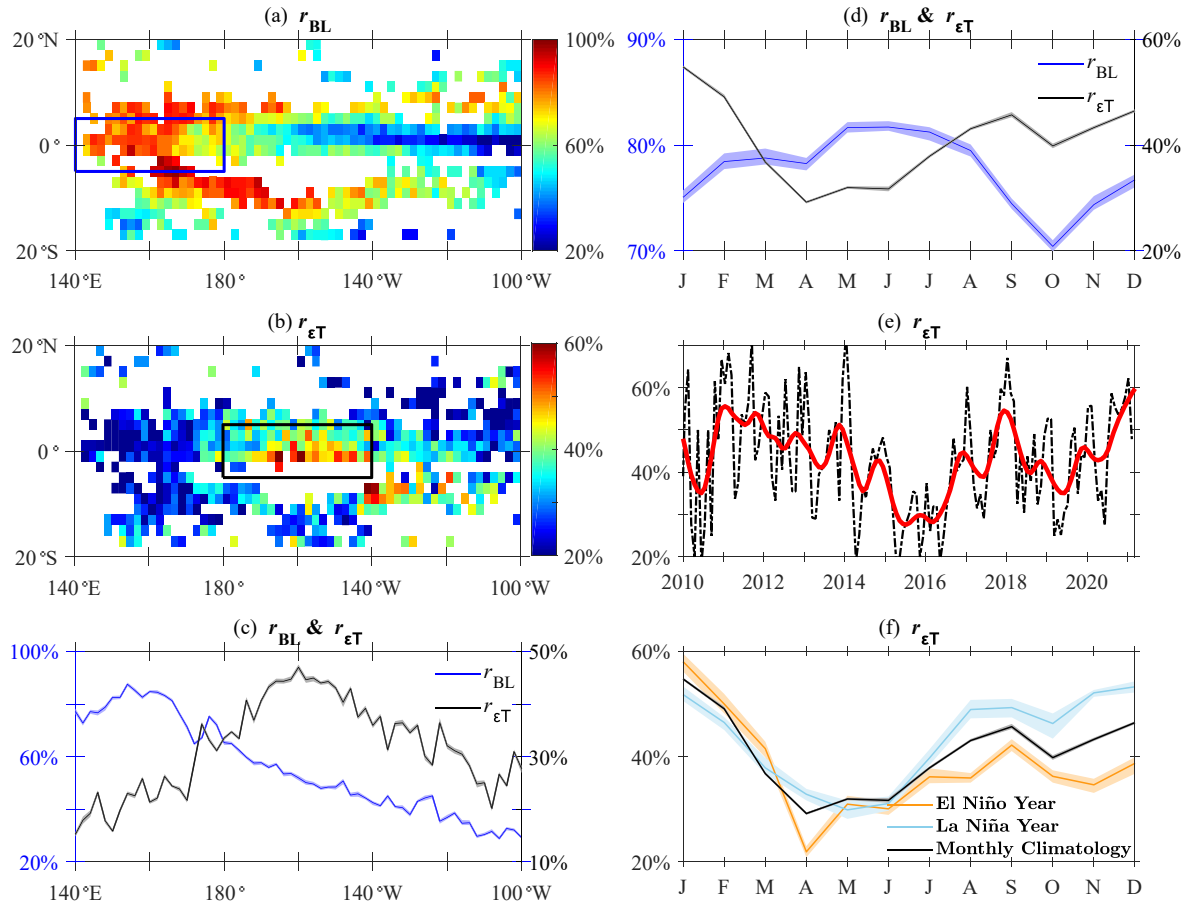

Figure 2. Argo-based estimates of (a) r_{BL} and (b) $r_{\varepsilon T}$ calculated over 2° × 2° boxes. (c) r_{BL} and $r_{\varepsilon T}$ calculated over 2° (longitude) × 10° (5°S–5°N) boxes, (d) monthly climatology of r_{BL} and $r_{\varepsilon T}$, (e) monthly $r_{\varepsilon T}$ (black dashed) with its 13-month running mean (red), and (f) monthly $r_{\varepsilon T}$ for El Niño, La Niña and all years. In (d)–(f), r_{BL} and $r_{\varepsilon T}$ are calculated over 140°E–180°, 5°S–5°N (box in a) and 180°–140°W, 5°S–5°N (box in b), respectively; shading denotes 95% bootstrap confidence levels. The interannual variation-associated stds for the mean values in f are within 5%–20% (not shown).

The Argo profiles disclosed extensive BL mixing events (Figure 2b). Spatially, $r_{\varepsilon T}$ varies between 20% and 60%, with high values in the central equatorial Pacific (between 180° and 140°W, 5°S–5°N, with an average $r_{\varepsilon T}$ of 41% and the maximum at approximately 160°W) (Figures 2b and 2c). Note that the hotspot of BL mixing is not consistent with that of BL. There is also an off-equatorial region in the southeastern Pacific that has high $r_{\varepsilon T}$, that is, 140°–110°W, 10°–5°S.

As mentioned above, the temporal variations of $r_{\varepsilon T}$ could have significant influence on the development of El Niño and should be identified. As a metric, the region 180°–140°W, 5°S–5°N (black box in Figure 2b) is selected to calculate the monthly climatology of $r_{\varepsilon T}$ (Figures 2d and 2e). Clearly, $r_{\varepsilon T}$ shows seasonal variations, with its maximum in boreal winter ($r_{\varepsilon T} > 55\%$ in January) and minimum in boreal spring ($r_{\varepsilon T} \approx 30\%$ in April). On the ENSO-focused interannual timescale (2–7-year period), $r_{\varepsilon T}$ reaches extrema at the end of 2010, 2017, and 2020 (La Niña years) and a long-term minimum at the end of 2015 (an El Niño year; Figure 2e); the correlation between the 13-month running mean of $r_{\varepsilon T}$ and Oceanic Nino Index (ONI) is -0.60 (CI = $[-0.69 \quad -0.48]$, $p \ll 0.001$), suggesting potential relationship to El Niño and La Niña conditions. We further calculated the monthly composite $r_{\varepsilon T}$ over El Niño (2014, 2015, 2018) and La Niña years (2010, 2011, 2016, 2017, 2020), respectively. It shows that, from July to December, $r_{\varepsilon T}$ is distinctly larger during La Niña than that of El Niño years (Figure 2f). Based on Maes et al. (2005)'s study, the regular interannual variation of $r_{\varepsilon T}$ may potentially impacts the evolution of El Niño and La Niña cycles. However, the differences between El Niño and La Niña years in January to June is not recognizable. More discussions on the effects of the interannual variation of $r_{\varepsilon T}$ will be presented in the last section.

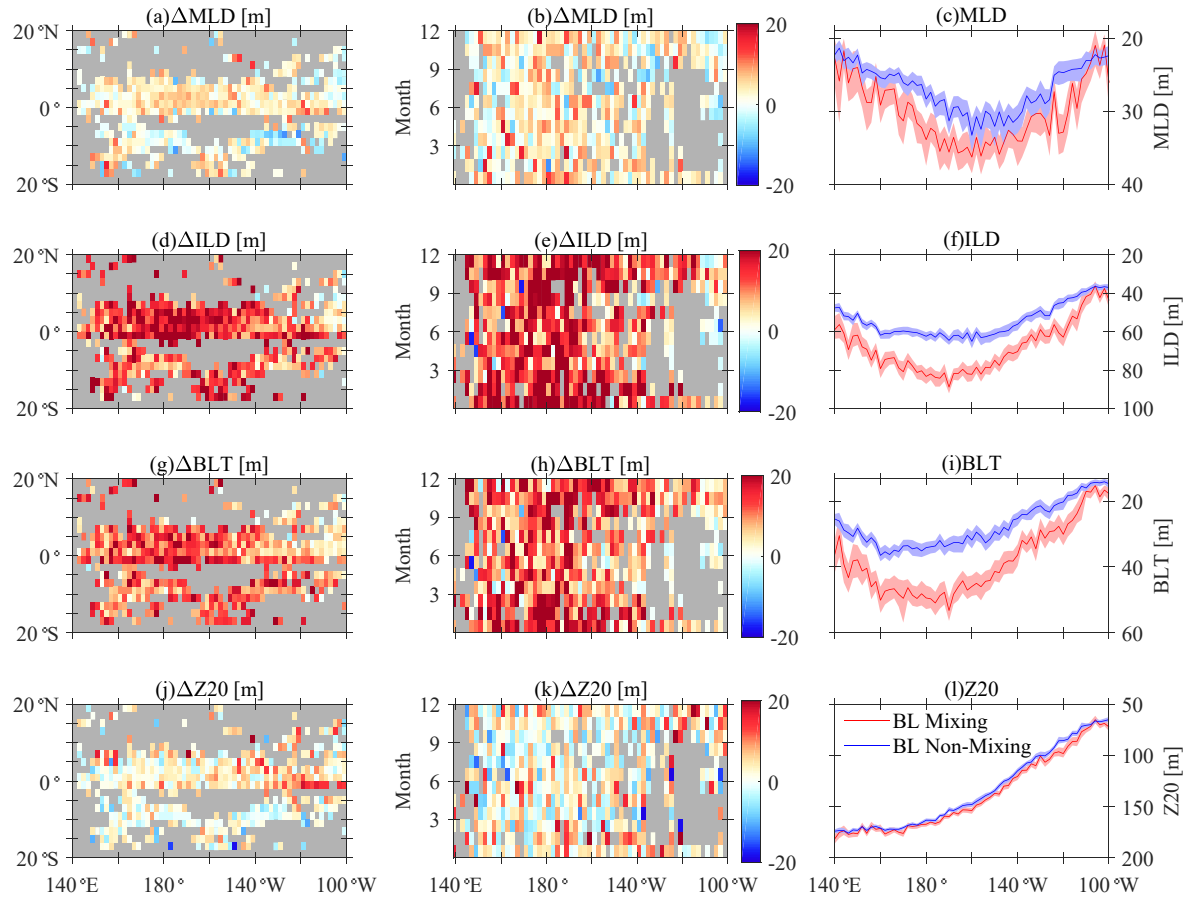

Figure 3. Differences between ocean states with and without mixing in BL. left: averaged over 2° × 2° boxes (the gray region denotes Argo profile samples less than 50); middle: longitude-month distributions (gray denotes BL profile samples ≤30); right: averaged over 2° (longitude) ×10° (5°S–5°N) boxes. (a–c) ML depth; (d–f) IL depth; (g–i) BL thickness; (j–l) depth of 20°C isotherm. In the right column, shading denotes the 95% bootstrap confidence limit.

3.3. BL Mixing and ML/IL/BL Thickening, Surface Layer Cooling, Salting, and BL Weakening

Now we examine what ocean states the BL mixing may associate with, from the basin-wide pattern and long-term mean perspectives. We first calculate the mean of the ML depths, IL depths, and the BL thickness (hereafter BLT) for the profiles with and without BL mixing, respectively, and then calculate their differences (Figure 3). Compared to those of BL nonmixing conditions, the ocean with BL mixing are associated with obviously increased ML and IL depths, and increased BLT over most of the equatorial Pacific (150°E−110°W, 10°S–10°N) (Figures 3a, 3d and 3g). The increments are large in the central equatorial Pacific (170°E−150°W), where the ML, IL, and BLT are increased up to 10, 25, and 20 m, respectively (Figures 3c, 3f and 3i). Note that, the correspondence between BL mixing and increased ML, IL, and BLT retain almost in all months, and shows only weak seasonal variations (Figures 3b, 3e and 3h).

We then investigate the differences in temperature, salinity in the IL, and vertical stratification (represented by N^2) in the BL (Figure 4). The results show that BL mixing is associated with significantly lower temperatures in the IL relative to BL nonmixing, with difference of −0.5°C on average and −2.0°C at maximum (Figures 4a and 4c). The differences over the MLs are the same (not shown). Large temperature differences occur also in the central equatorial Pacific (170°E−150°W, 10°S–10°N). They are also associated with significantly higher salinity, with differences of 0.1 PSU on average and 0.2 PSU at maximum (Figures 4d and 4f). The BL mixing is associated with weaker stratification of the BLs compared to BL nonmixing, with the mean difference being approximately $-0.5 \times 10^{-4} s^{-2}$, and reaching up to $-0.8 \times 10^{-4} s^{-2}$ (Figures 4g and 4i). Large stratification differences mainly occur in the western-central equatorial Pacific (155°E−160°W, 10°S–10°N). Similarly, the pattern

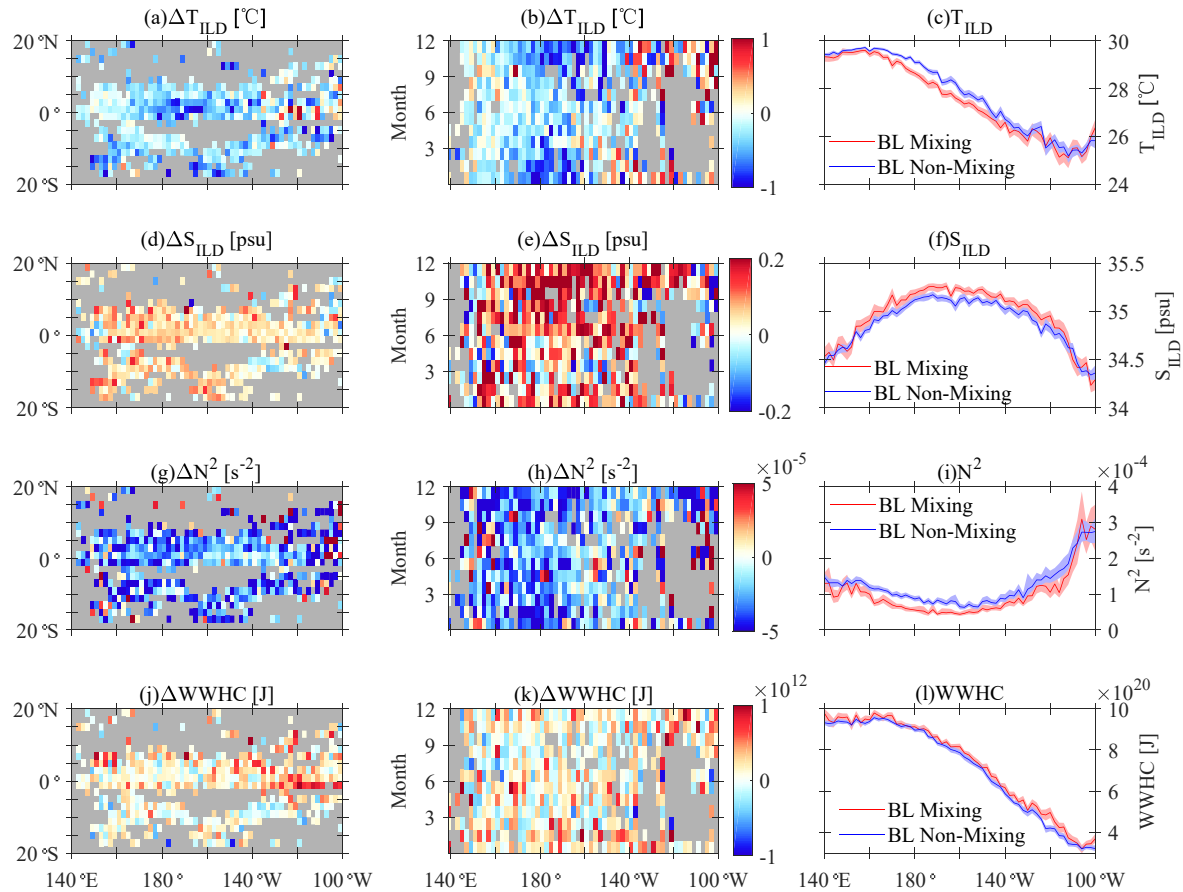

Figure 4. The same as Figure 3, but for (a–c) temperature and (d–f) salinity at the ILD, (g–i) stratification over the BL and (j–l) warmer water heat content, that is heat content above 20°C depth, respectively.

of difference in temperature, salinity, and stratification remains almost the same for each month, though weak seasonal variations are displayed (Figures 4b, 4e and 4h).

As reviewed above, a factor that is of high significance, particularly for the El Niño development, is the WWV or the warm water heat content (WWHC), which is represented by the water volume or heat content above the 20° isothermal (Z20). It is found that the BL mixing is associated with slightly larger Z20, mostly less than 10 m (Figures 3j, k and 3l), and with slightly less but insignificant WWHC (Figures 4j, k and 4l). The implications of the BL mixing and the associated ocean state changes for ENSO development is indirect and will be discussed in the last section.

4. Summary and Discussion

In this letter, we first report on strong mixing in the BL based on two 3-day-long direct turbulence measurements in the western equatorial Pacific. The BL mixing yielded effective heat transfer across the BL and the thermocline. We notice that BL mixing has also been observed by few previous turbulence measurements in the western equatorial Pacific, although it was not a focus of those studies. For example, Wijesekera and Gregg (1996) observed two cases of strong turbulent mixing which penetrated well below the ML and till approximately 100 m during the Tropical Ocean-Global Atmosphere-Coupled Ocean Atmosphere Response Experiment (TOGA-COARE) project (11 November to 3 December 1992) at 156°E, 1°43′S.

Next, we employ the Thorpe Scale method and the Argo profile data to find BL mixing events (i.e., density inversions, but not mixing coefficients) in the equatorial Pacific, which resolves the intermittency and sparseness of BL mixing observations. We show that the occurrence rate of BL mixing ranges between 20% and 60%,

higher in the central equatorial Pacific (180°E–140°W, 5°S–5°N) with the maximum near 160°W, 0°. There, BL mixing occurs most (least) frequently in winter (spring), and more frequently in mature La Niña than mature El Niño conditions. The results are, to our knowledge, the first data-based identification of BL mixing in the wide equatorial Pacific basin.

We then investigate the conditions that favor the occurrence of BL mixing. Compared to ocean states without BL mixing, the BL mixing is associated with increased ML, IL, and BLT, with the difference reaching up to 10, 25, and 20 m, respectively, in the central equatorial Pacific. They are also associated with significant cooling and salting in both the MLs and ILs, and weaker stratification in the BLs. It is noticeable that the relationships between BL stratification and surface temperature and salinity are consistent with Maes and O'Kane (2014), who found the ocean salinity stratification above the main pycnocline is quasi-linearly positively (negatively) related with the surface temperature (salinity).

The generation mechanism for the BL mixing remains unrevealed and beyond the scope of this brief Letter. However, the weaker stratification (with cooler and saltier upper layer water) seen in profiles with BL mixing certainly is favorable for generation of the mixing. In turn, the BL mixing may weaken the stratification of the BL. The interplay between those processes leads to subtle causal relationship between the BL mixing and the ocean properties, which needs to be verified by future studies. At least, it can be envisioned that if the BL mixing is strong enough, the BL may be enlarged or even destroyed; in this sense, the BL mixing should be considered as an important mechanism for the BL's annihilation and variation, which was already noticed with numerical model outputs (Gao et al., 2014).

Given that the BL mixing is organized in distinct annual and interannual cycles, and occurs not only in the Western Pacific warm pool, but also in the central equatorial Pacific, its large-scale effect is highly worthy of further exploring. Whether or how the real BL mixing, hotspot of which is notably inconsistent with that of the BLs, may weaken or even block an El Niño event, could be different from the conclusions obtained from Maes et al.'s sensitivity studies (Maes et al., 2002; 2005; Maes and Belamari, 2011), in that the latter adopted artificially prescribed super strong BL mixing on specific region and time—it is even unclear if the BL mixing's influence occurs through the same physical mechanisms. It indicates that both the BL and BL mixing should be well resolved/represented for the numerical models to better simulate and predict ENSO (Jia et al., 2021; Warner and Moum, 2019; Wengel et al., 2021).

Data Availability Statement

The observational data is available at https://zenodo.org/record/5813557#.YdG-uW5uKzk. The Argo data were collected and made freely available by the International Argo Program and the national programs that contribute to it (https://www.ocean-ops.org); the Argo Program is part of the Global Ocean Observing System; and the general Argo DOI is https://doi.org/10.17882/42182. The ASCAT data is available at http://doi.org/10.15770/EUM_SAF_OSI_0006. Those data are highly appreciated.

Acknowledgments
This study is supported by the Strategic Priority Research Program of Chinese Academy of Sciences (CAS) (XDB42000000), the Key Research Program of Frontier Sciences of CAS (QYZDB-SSW-DQC030), and the National Natural Science Foundation of China (NSFC 41976012, 41806015, 42090044, 91858201). Fan Wang is funded by NSFC under No. 41730534. Thanks to X. Zhou and crew of R/V "Kexue" for conducting the turbulence measurements.

References

Ando, K., & McPhaden, M. J. (1997). Variability of surface layer hydrography in the tropical Pacific Ocean. *Journal of Geophysical Research - C: Oceans*, *102*(C10), 23063–23078. https://doi.org/10.1029/97JC01443

Bosc, C., Delcroix, T., & Maes, C. (2009). Barrier layer variability in the western Pacific warm pool from 2000 to 2007. *Journal of Geophysical Research: Oceans*, *114*(6), 1–14. https://doi.org/10.1029/2008JC005187

de Boyer Montégut, C., Madec, G., Fischer, A. S., Lazar, A., & Iudicone, D. (2004). Mixed layer depth over the global ocean: An examination of profile data and a profile-based climatology. *Journal of Geophysical Research - C: Oceans*, *109*(12), 1–20. https://doi.org/10.1029/2004JC002378

Corbett, C. M., Subrahmanyam, B., & Giese, B. S. (2017). A comparison of sea surface salinity in the equatorial Pacific Ocean during the 1997–1998, 2012–2013, and 2014–2015 enso events. *Climate Dynamics*, *49*(9-10), 1-14.

Delcroix, T., Eldin, G., Radenac, M.-H., Toole, J., & Firing, E. (1992). Variation of the western equatorial Pacific Ocean, 1986–1988. *Journal of Geophysical Research*, *97*(C4), 5423. https://doi.org/10.1029/92jc00127

Gao, S., Qu, T., & Nie, X. (2014). Mixed layer salinity budget in the tropical Pacific Ocean estimated by a global GCM. *Journal of Geophysical Research: Oceans*, *119*(12), 8255–8270.

Guan, C., Hu, S., Mcphaden, M. J., Wang, F., Gao, S., & Hou, Y. (2019). Dipole Structure of Mixed Layer Salinity in Response to El Nio-La Nia Asymmetry in the Tropical Pacific. *Geophysical Research Letters*, *46*(21).

Jia, Y., Richards, K. J., & Annamalai, H. (2021). The impact of vertical resolution in reducing biases in sea surface temperature in a tropical Pacific Ocean model. *Ocean Modelling*, *157*, 101722.

Jin, F. F. (1997). An equatorial ocean recharge paradigm for ENSO. Part I: Conceptual model. *Journal of the Atmospheric Sciences*, *54*(7), 811–829. https://doi.org/10.1175/1520-0469(1997)054<0811:AEORPF>2.0.CO

Lukas, R., & Lindstrom, E. (1991). The mixed layer of the western equatorial Pacific Ocean. *Journal of Geophysical Research*, *96*(S01), 3343. https://doi.org/10.1029/90jc01951

Maes, C., & Belamari, S. (2011). On the impact of salinity barrier layer on the Pacific Ocean mean state and ENSO. *Scientific Online Letters on the Atmosphere*, *7*(1), 97–100. https://doi.org/10.2151/sola.2011-025

Maes, C., Delecluse, P., & Madec, G. (1997). Impact of westerly wind bursts on the warm pool of the TOGA-COARE domain in an OGCM. *Climate Dynamics*, *14*, 55–70. https://doi.org/10.1007/s003820050208

Maes, C., & O'Kane, T. J. (2014). Seasonal variations of the upper ocean salinity stratification in the Tropics. *Journal of Geophysical Research: Oceans*, *119*, 1706–1722. https://doi.org/10.1002/2013JC009366

Maes, C., Picaut, J., & Belamari, S. (2002). Salinity barrier layer and onset of El Niño in a Pacific coupled model. *Geophysical Research Letters*, *29*(24), 2–5. https://doi.org/10.1029/2002GL016029

Maes, C., Picaut, J., & Belamari, S. (2005). Importance of the salinity barrier layer for the buildup of El Niño. *Journal of Climate*, *18*(1), 104–118. https://doi.org/10.1175/JCLI-3214.1

McPhaden, M. J. (2002). Mixed layer temperature balance on intraseasonal timescales in the equatorial Pacific Ocean. *Journal of Climate*, *15*(18), 2632–2647. https://doi.org/10.1175/1520-0442(2002)015<2632:MLTBOI>2.0.CO

Meinen, C. S., & McPhaden, M. J. (2000). Observations of warm water volume changes in the equatorial Pacific and their relationship to El Nino and La Nina. *Journal of Climate*, *13*(20), 3551–3559. https://doi.org/10.1175/1520-0442(2000)013<3551:OOWWVC>2.0.CO

Osborn, T. R. (1980). Estimates of the local rate of vertical diffusion from dissipation measurements. *Journal of Physical Oceanography 10*(1). 83-89. https://doi.org/10.1175/1520-0485(1980)010<0083:EOTLRO>2.0.CO;2

Qu, T., Song, Y.T., & Maes, C. (2014). Sea surface salinity and barrier layer variability in the equatorial Pacific as seen from Aquarius and Argo. *Journal of Geophysical Research: Oceans*, *119*, 15-29.

Schneider, N., & Muller, P. (1990). The meridional and seasonal structures of the mixed layer depth and its diurnal amplitude observed during the Hawaii to Tahiti Shuttle Experiment. *Journal of Physical Oceanography*, *20*, 1395–1404.

Sprintall, J., & Tomczak, M. (1992). Evidence of the Barrier Layer in the Surface Layer of the Tropics ocean surface mixed layer generally denotes a quasi- kinetic energy and potential energy processes mentioned its degree state. *Journal of Geophysical Research*, *97*(C5), 7305–7316.

Thorpe, S. A. (1977). Turbulence and mixing in a Scottish Loch. *Philosophical Transactions of the Royal Society A: Mathematical, Physical & Engineering Sciences*, *286*(1334), 125–181. https://doi.org/10.1098/rsta.1977.0112

Vialard, J., & Delecluse, P. (1998a). An OGCM study for the TOGA decade. Part I: Role of salinity in the physics of the western Pacific fresh pool. *Journal of Physical Oceanography*, *28*(6), 1071–1088. Retrieved from http://www.scopus.com/inward/record.url?eid=2-s2.0-0032443482&partnerID=tZOtx3y1

Vialard, J., & Delecluse, P. (1998b). An OGCM study for the TOGA decade. Part II: Barrier-layer formation and variability. *Journal of Physical Oceanography*, *28*(6), 10892–11106. https://doi.org/10.1175/1520-0485(1998)028<1089:AOSFTT>2.0.CO

Vialard, J., Delecluse, P., & Menkes, C. (2002). A modeling study of salinity variability and its effects in the tropical Pacific Ocean during the 1993-1999 period. *Journal of Geophysical Research: Oceans*, *107*(12). https://doi.org/10.1029/2000jc000758

Vialard, J., Menkes, C., Boulanger, J. P., Delecluse, P., Guilyardi, E., McPhaden, M. J., & Madec, G. (2001). A model study of oceanic mechanisms affecting equatorial pacific sea surface temperature during the 1997-98 El Niño. *Journal of Physical Oceanography* (Vol. *31*, 7 pp. 1649–1675). https://doi.org/10.1175/1520-0485(2001)031<1649:AMSOOM>2.0.CO;2

Warner, S. J., & Moum, J. N. (2019). Feedback of mixing to enso phase change. *Geophysical Research Letters*, *46*(23).

Wengel, C., Lee, S.S., Stuecker, M.F., Timmermann, A., Chu, J.-E., & Schloesser, F., (2021). Future high-resolution El Niño/Southern Oscillation dynamics. *Nature Climate Change*. *11*, 758–765.

Whalen, C. B., MacKinnon, J. A., & Talley, L. D. (2018). Large-scale impacts of the mesoscale environment on mixing from wind-driven internal waves. *Nature Geoscience*, *11*(11), 842–847. https://doi.org/10.1038/s41561-018-0213-6

Wijesekera, H. W., & Gregg, M. C. (1996). Surface layer response to weak winds, westerly bursts, and rain squalls in the western Pacific Warm Pool. *Journal of Geophysical Research - C: Oceans*, *101*(C1), 977–997. https://doi.org/10.1029/95JC02553

Wyrtki, K. (1975). El Niño—the dynamic response of the equatorial pacific Oceanto atmospheric forcing. *Journal of Physical Oceanography*, *5*(4), 572–584. https://doi.org/10.1175/1520-0485(1975)005<0572:entdro>2.0.co;2

Zheng, F., Zhang, R.-H., & Zhu, J. (2014). Effects of interannual salinity variability on the barrier layer in the western-central equatorial pacific: A diagnostic analysis from Argo. *Advances in Atmospheric Sciences*, *31*(3), 532–542.